

Multipole quantum droplets in quasi-one-dimensional asymmetric mixtures

Yaroslav V. Kartashov¹ and Dmitry A. Zezyulin²

¹*Institute of Spectroscopy, Russian Academy of Sciences, Troitsk, Moscow 108840, Russia*

²*School of Physics and Engineering, ITMO University, St. Petersburg 197101, Russia*



(Received 9 July 2024; accepted 19 August 2024; published 28 August 2024)

We study quantum droplets emerging in a quasi-one-dimensional asymmetric mixture of two atomic species with different intracomponent coupling constants. We find that such mixtures support a rich variety of multipole quantum droplets, where the macroscopic wave function of one component changes its sign and features a distinctive multipole structure, while the wave function of another component does not have zeros. Such multipole droplets have no counterparts in the reduced single-component model frequently used to describe symmetric one-dimensional mixtures. We study transformations of multipole states upon variation of the chemical potential of each component and demonstrate that quantum droplets can split into separated fundamental states, transform into flattop multipoles, or into a multipole component coupled to a flattop state with several humps on it, akin to antidark solitons. Multipole quantum droplets described here are stable in a large part of their existence domain. Our findings essentially broaden the family of quantum droplet states emerging in the beyond-mean-field regime and open the way for observation of such heterostructured states in Bose-Bose mixtures.

DOI: [10.1103/PhysRevA.110.L021304](https://doi.org/10.1103/PhysRevA.110.L021304)

Introduction. Quantum droplets (QDs) in Bose-Bose mixtures emerge due to the balance between mean-field interactions and the Lee-Huang-Yang (LHY) correction [1] to the mean-field energy [2]. An important peculiarity of QDs stems from different roles played by the LHY correction in settings of different dimensionality. For example, in the three-dimensional (3D) case LHY correction provides the repulsive effect and stabilizes the atomic mixture against the mean-field collapse, while in effectively one-dimensional (1D) mixtures [3–5] the LHY correction corresponds to effective attraction, compensating the intraspecies repulsion and enabling the formation of self-bound states even in free space [3]. Competition between mean-field and LHY nonlinearities leads to very unusual shape transformations and stability properties of QDs. Experimentally, QDs have been observed in dipolar Bose-Einstein condensates [6–11], as well as in Bose-Bose mixtures consisting of atoms in different hyperfine states, which are characterized by unequal coupling constants [12–15], and in heteronuclear Bose-Bose mixtures characterized by different atomic masses in two species [16,17]. Current progress in experiments with QDs and their theoretical treatment is described in recent reviews [18,19].

Theoretical description of Bose-Bose mixtures frequently assumes a symmetric mixture of two species with equal atomic masses and intracomponent coupling constants allowing to derive a reduced single-component model, where both species are described by the same Gross-Pitaevskii-like equation [3,20–26]. At the same time, this assumption drastically limits the set of available nonlinear states. For this reason, the exploration of new types of QDs in essentially *two-component* and *asymmetric* mixtures becomes particularly important, as this situation is most frequently encountered in experiments. Besides simple transformation of shapes of QD components encountered in asymmetric mixtures [27], it was found that

asymmetry can lead to instabilities and new types of states [28–31] that do not appear in the scalar case. The variety of stable QDs is particularly rich in multidimensional settings, where LHY correction can stabilize not only fundamental [12–17] but also excited states, such as vortical and rotating QDs [32–38]. External trapping potentials [24,39,40] and periodic lattices [41–51] further enrich the structure and evolution regimes of QDs.

Surprisingly, when it comes to 1D QDs, only the simplest fundamental (i.e., nodeless) asymmetric states have been reported so far in settings without lattices or other types of confining potentials. In this Letter, we show that the family of 1D QDs in asymmetric mixtures in free space is in fact much richer and includes stable multipole states which do not have counterparts in the one-component system. In particular, we present the families of dipole and tripole QDs, identify the ranges of their existence and stability on the plane of chemical potentials of both species, and demonstrate that such QDs exhibit rich shape transformations within their existence domains, ranging from transformation of multipole QDs into several separated fundamental states, to flattop multipoles, or multipoles coupled with humps on a localized flattop plateau, resembling antidark states.

Model. We study an asymmetric quasi-1D Bose-Bose mixture, where both species have equal atomic masses, but different intraspecies coupling constants. This situation corresponds, for example, to experiments with a mixture of ³⁹K atoms in different hyperfine states [12–15]. Evolution of dimensionless wave functions $\psi_{1,2}(x, t)$ is governed by the system [3,30,52]

$$i \frac{\partial \psi_{1,2}}{\partial t} = -\frac{1}{2} \frac{\partial^2 \psi_{1,2}}{\partial x^2} + \frac{\partial E(n_1, n_2)}{\partial n_{1,2}} \psi_{1,2}, \quad (1)$$

where $n_{1,2} = |\psi_{1,2}|^2$ and the energy density reads

$$E(n_1, n_2) = \frac{(g_1^{1/2}n_1 - g_2^{1/2}n_2)^2}{2} - \frac{2}{3\pi}(g_1n_1 + g_2n_2)^{3/2} + \frac{\delta(g_1g_2)^{1/2}}{(g_1 + g_2)^2}(g_1^{1/2}n_2 + g_2^{1/2}n_1)^2. \quad (2)$$

Dimensionless coefficients $g_{1,2} > 0$ characterize intraspecies interactions in each component, coefficient $g_{12} < 0$ defines interspecies interactions, and $\delta = g_{12} + (g_1g_2)^{1/2}$. In experiments δ is positive and small. In our simulations we use [30] $g_1 = 0.639$, $g_2 = 2.269$, and $g_{12} = -1$ that corresponds to $\delta \approx 0.204$.

We search for asymmetric stationary states with generically different chemical potentials and spatial profiles $\psi_{1,2} = e^{-i\mu_{1,2}t}u_{1,2}(x)$, where the functions $u_{1,2}$ are real-valued and localized, i.e., $u_{1,2} \rightarrow 0$ as $x \rightarrow \pm\infty$. The system (1) is known to support fundamental (or monopole) droplets, where both functions $u_{1,2}(x)$ are nodeless [27]. In contrast, here we introduce *multipole* droplets, where one of the functions $u_{1,2}(x)$ can have zeros. Specifically, we focus on dipole and tripole solutions, in which the first component u_1 has one or two zeros, respectively, while the second component u_2 is nodeless. Such solutions can be obtained from Eq. (1) using Newton's method with a suitable initial guess, which is necessary for

numerical iterations to converge to a multipole state and not to a ground-state monopole one. We used initial guesses in the form of a superposition of two or three (for dipoles and tripoles, respectively) well-separated sech-shaped profiles which were taken with the same sign in the second component and with alternating signs in the first component.

Classification of solutions. First, we briefly describe the most important properties of a single-component model, which can be formally obtained from (1) by setting the wave function of the first species to zero, i.e., $u_1 \equiv 0$. Then, the problem reduces to a single equation for $u_2(x)$ that has only monopole single-component solutions existing for chemical potential μ_2 in the interval $\mu_2^{co} < \mu_2 < 0$, where the cutoff (co) value is given by

$$\mu_2^{co} := \partial E(0, n_2^{co})/\partial n_2, \quad (3)$$

and the limiting density n_2^{co} can be determined from the condition

$$\partial E(0, n_2^{co})/\partial n_2 = E(0, n_2^{co})/n_2^{co}. \quad (4)$$

It is well known [3,20] that as μ_2 approaches μ_2^{co} from the right, the solution $u_2(x)$ develops the flattop shape, while $\max(n_2) \rightarrow n_2^{co}$. Irrespective of the number of condensed atoms, the density $n_2(x)$ does not exceed n_2^{co} . As a result, the droplet drastically broadens, and the number of atoms diverges as μ_2 approaches the cutoff value from the right: $\lim_{\mu_2 \rightarrow \mu_2^{co}+0} N_2 = \infty$, where by definition $N_{1,2} = \int_{-\infty}^{\infty} |\psi_{1,2}|^2 dx$. When $\mu_2 \rightarrow 0$, the norm N_2 vanishes. For the

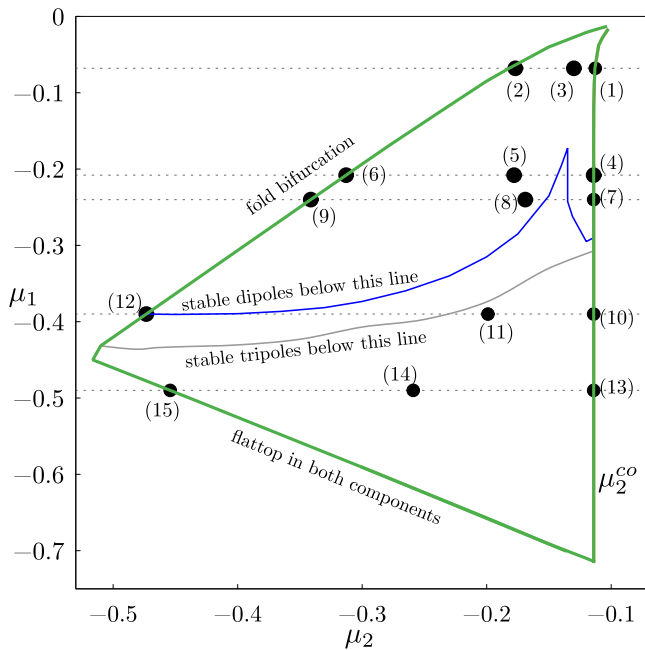


FIG. 1. The nearly triangular area illustrates the existence domain for dipole and tripole QDs on the plane of chemical potentials (μ_1, μ_2) . The right boundary of the triangle corresponds to the cutoff value $\mu_2 = \mu_2^{co}$ of the single-component solution $(0, \psi_2)$. At the upper boundary of the triangle dipole and tripole solutions undergo fold bifurcation, and at the lower boundary they transform into flattop multipoles. Enumerated circles correspond to specific solutions whose profiles are shown in Figs. 3 and 4. The diagram displays two stability boundaries, with dipole and tripole QDs being stable below the corresponding boundary. In this and subsequent figures all plotted quantities are dimensionless.

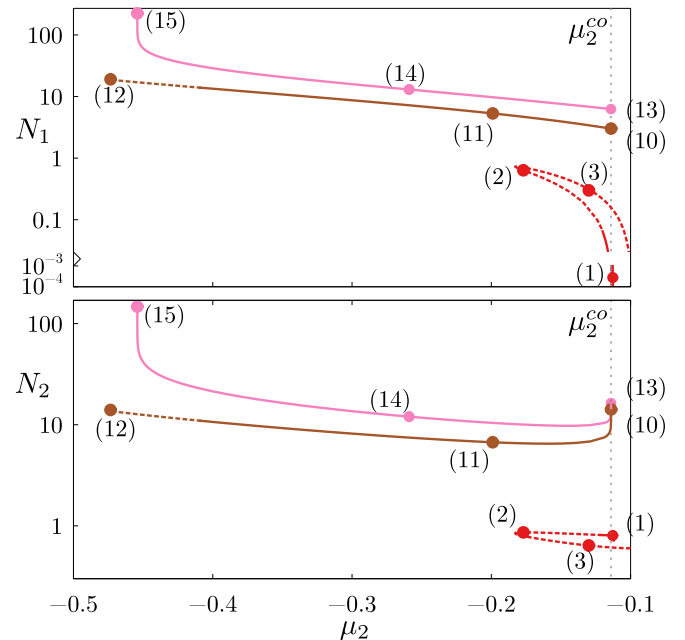


FIG. 2. Number of particles in the first (upper panel) and second (lower panel) component vs μ_2 for fixed μ_1 . Only dipole solutions are shown in this figure. Solid and dashed fragments correspond to stable and unstable solutions, respectively. Enumerated circles correspond to solutions marked in the existence diagram in Fig. 1 and plotted in Figs. 3 and 4. Red, brown, and pink lines correspond to $\mu_1 = -0.068$, $\mu_1 = -0.39$, and $\mu_1 = -0.49$, respectively.

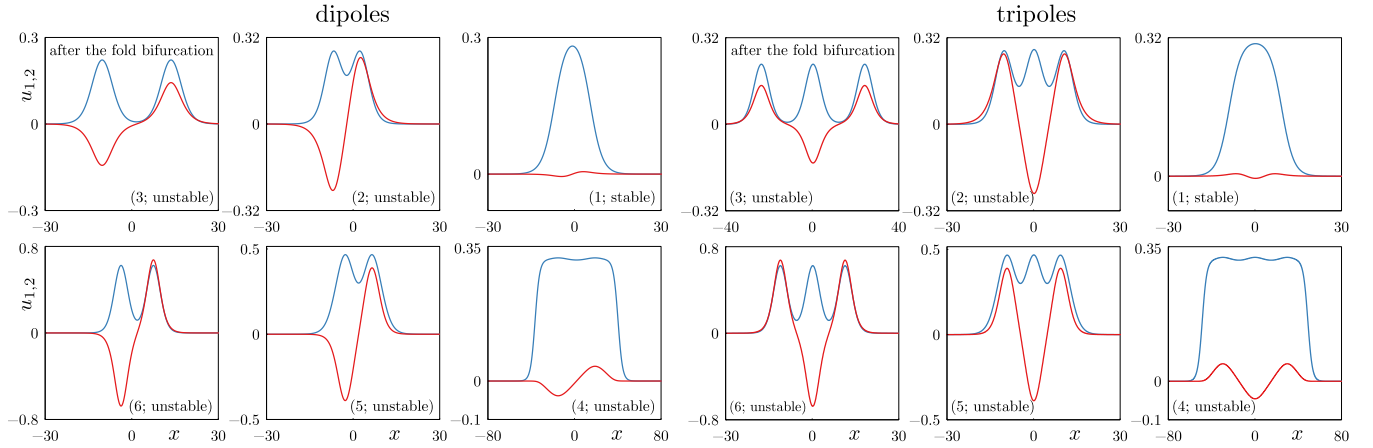


FIG. 3. Profiles $u_{1,2}(x)$ of two components of dipole and tripole QDs that transform into a single-component state $(0, u_2)$ at the right boundary of the triangular existence area. Red and blue lines correspond to the first and second components. Each row corresponds to the fixed value of μ_1 (see horizontal dashed lines in Fig. 1), while panels are enumerated in accordance with circles in the existence diagram in Fig. 1. Notice that solution 3 is situated after the fold bifurcation; see corresponding solution in Fig. 2.

one-component system one gets

$$u_2^{\text{co}} = 2g_2^{3/2}/(3\pi G_2) \quad \text{and} \quad \mu_2^{\text{co}} = -2g_2^3/(9\pi^2 G_2), \quad (5)$$

where $G_2 = g_2 + 2\delta g_1^{3/2} g_2^{1/2}/(g_1 + g_2)^2$. For coupling constants adopted in our study, Eqs. (5) yield $\mu_2^{\text{co}} \approx -0.114$ and $u_2^{\text{co}} \approx 0.315$. Remarkably, multipole two-component states described below exist with chemical potentials situated to the left of the region of existence of single-component states. Next, we proceed to the main part of our study devoted to two-component mixtures with $u_{1,2} \neq 0$. In Fig. 1 we illustrate the domain of existence of dipole and tripole solutions on the plane (μ_1, μ_2) , while in Fig. 2 we plot representative

dependencies of numbers of particles N_1 and N_2 on the chemical potential of the second species μ_2 for several fixed μ_1 values. Representative profiles of multipole QDs corresponding to the dots in Fig. 1 are displayed in Figs. 3 and 4.

Multipole states exist within the bounded domain on the (μ_1, μ_2) plane that has a nearly triangular shape (see Fig. 1). The right side of the triangle approximately coincides with the $\mu_2 = \mu_2^{\text{co}}$ value corresponding to the cutoff for single-component condensate introduced above in Eq. (5). We classify the found solutions in two groups which differ by their behavior near the right boundary of the existence area. As μ_2 approaches μ_2^{co} from the left, solutions of the first group transform into the single-component states $(0, u_2)$ briefly

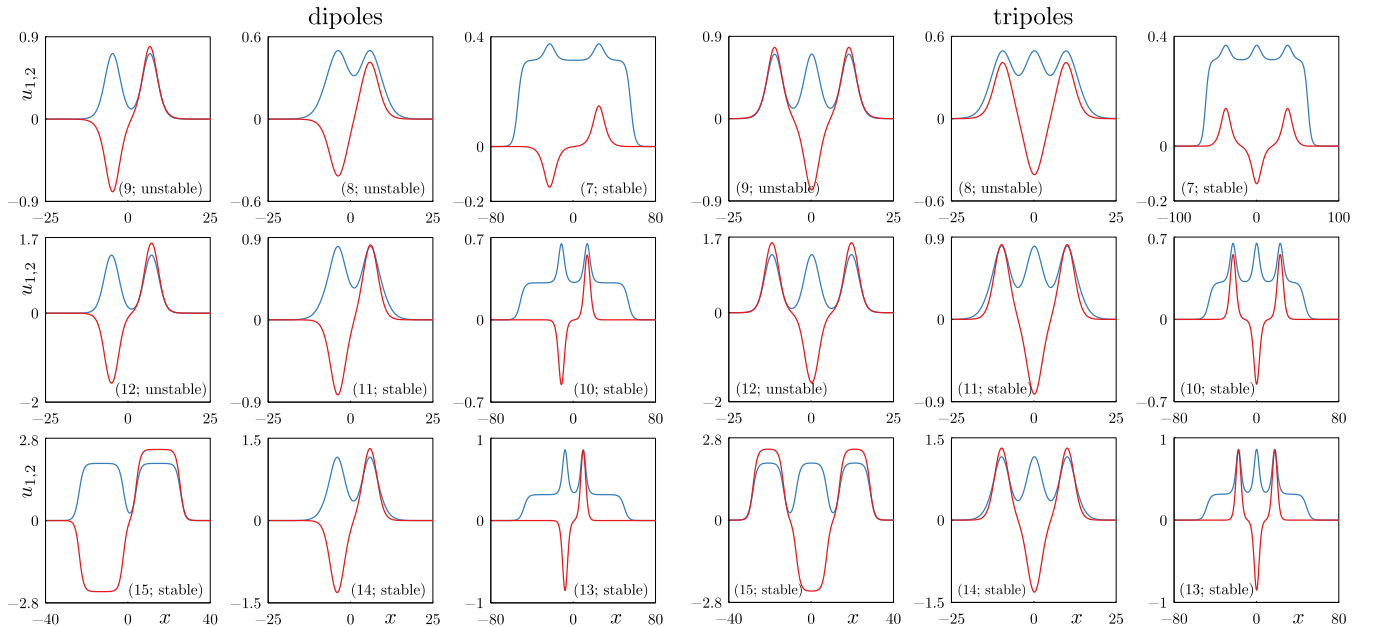


FIG. 4. Profiles $u_{1,2}(x)$ of dipole and tripole QDs that transform into a multipole state in one component coupled to the antidark state in other component at the right boundary of the triangular existence area. Red and blue lines correspond to the first and second components, respectively. Each row corresponds to the fixed value of μ_1 , and panels are enumerated in accordance with circles in the existence diagram in Fig. 1.

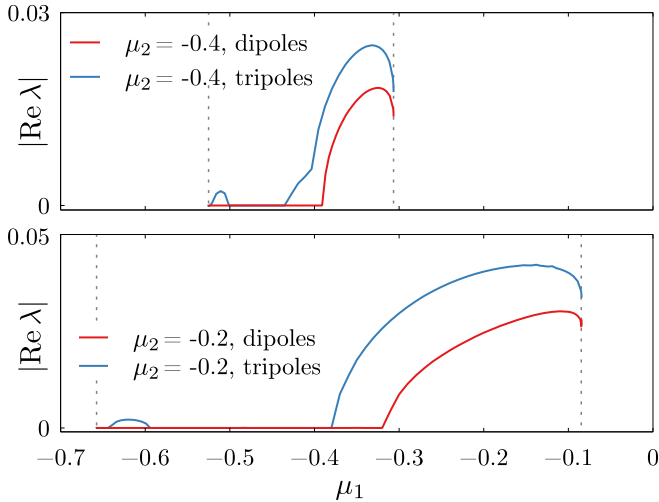


FIG. 5. Instability increments vs chemical potential of the first component μ_1 for dipole and tripole solutions at $\mu_2 = -0.2$ and $\mu_2 = -0.4$. Horizontal spans of plotted curves are limited by the existence intervals of corresponding solutions (and additionally highlighted with vertical dashed lines). Apart from relatively strong instability, tripole QDs also feature narrow bands of weak instabilities, with increments below 10^{-3} . These weak instabilities are not shown in the existence diagram in Fig. 1.

described above. Respectively, close to the right boundary of the existence area each solution of this type represents a localized nodeless state in the second component coupled to a small-amplitude multipole state in the first component; see examples shown in Fig. 3 (specifically, solutions with numbers 1 and 4). Each solution of this type can be continued by decreasing μ_2 , while keeping μ_1 fixed. This is accompanied by the increase of the amplitude of the first component, which eventually becomes comparable with the second component (see solutions 2 and 5 in Fig. 3). When μ_2 reaches the left side of the triangular existence area, a fold bifurcation takes place, i.e., the solution family makes a U-turn and continues toward *increasing* values of μ_2 . A representative example of this fold bifurcation is presented in Fig. 2 (see the red curves corresponding to $\mu_1 = -0.068$). After the fold bifurcation, with the increase of μ_2 such states gradually transform into well-separated sets of two (for dipoles) or three (for tripoles) fundamental QDs (see solutions with numbers 3 in Fig. 3 and the corresponding point in Fig. 2).

The second group of solutions (illustrated in Fig. 4) features different behavior near the right boundary of the existence domain. Such states transform into a structure that comprises two (for dipoles) or three (for tripoles) out-of-phase well-separated humps in the first component coupled to two (or three) in-phase humps situated on the flattop pedestal in the second component, akin to antidark states. Examples of such states are shown in Fig. 4 as solutions 7, 10, and 13. As μ_2 approaches the right boundary of the existence area, the distance between the out-of-phase (in-phase) humps in the first (second) component increases. Therefore, the number of particles diverges in the second component, but remains finite and nonzero in the first component. The difference between solutions from the first and second groups of solutions is best visible in the $N_1(\mu_2)$ dependencies plotted in upper panel of

Fig. 2. For solutions of the first group the number of particles N_1 vanishes at $\mu_2 \rightarrow \mu_2^{\text{co}}$ [see point 1 in Fig. 2(a)], while for solutions of the second group N_1 remains nonzero [points 10 and 13 in Fig. 2(a)]. As μ_2 decreases, the behavior of QDs from the second group can be different depending on the value of chemical potential μ_1 of the first component. If the branch of solutions reaches the left upper boundary of the triangle (see solutions 9 and 12 in Figs. 1 and 4), then fold bifurcation takes place, by analogy with states from the first group. In contrast, if μ_1 is such that the family of states reaches the lower left border of the triangle, then both components develop flattop shapes, while a multipole structure is maintained (see dipole and tripole solutions 15 in Figs. 1 and 4). We note that the boundaries of the existence domain on the (μ_1, μ_2) plane for dipole and tripole QDs are identical.

Boundaries of the existence area in Fig. 1 show a different response to the change of intraspecies coupling coefficient g_{12} (and, respectively, to the change of auxiliary coefficient δ). Changing g_{12} in the range from -1.05 to -0.95 (resp., $0.15 \lesssim \delta \lesssim 0.25$), we found that the boundary corresponding to fold bifurcations does not change appreciably, while the boundary corresponding to the flattop shape in both components does change: for smaller values of δ the flattop regime is achieved at smaller negative values of μ_1 and μ_2 , i.e., the existence area broadens, and *vice versa*, the increase of δ makes the existence domain narrower.

Stability. To examine the stability of multipole droplets, we use linear stability analysis and systematic dynamical simulations. For linear stability, we take perturbed stationary solution $\psi_{1,2} = e^{-i\mu_{1,2}t}[u_{1,2}(x) + \eta_{1,2}(x, t)]$, where $\eta_{1,2}$ are small perturbations. With representation $\eta_{1,2}(x, t) = [P_{1,2}(x) + Q_{1,2}(x)]e^{\lambda t} + [P_{1,2}^*(x) - Q_{1,2}^*(x)]e^{\lambda^*t}$, the standard linearization procedure leads to the eigenvalue problem

$$i\lambda P_{1,2} = \left[-\frac{1}{2} \frac{d^2}{dx^2} - \mu_{1,2} + \frac{\partial E}{\partial n_{1,2}} \right] Q_{1,2}, \quad (6)$$

$$i\lambda Q_{1,2} = \left[-\frac{1}{2} \frac{d^2}{dx^2} - \mu_{1,2} + \frac{\partial E}{\partial n_{1,2}} + 2u_{1,2}^2 \frac{\partial^2 E}{\partial n_{1,2}^2} \right] P_{1,2} + 2u_1 u_2 \frac{\partial^2 E}{\partial n_1 \partial n_2} P_{2,1}, \quad (7)$$

where partial derivatives of $E(n_1, n_2)$ are evaluated at $n_{1,2} = u_{1,2}^2(x)$. This problem has been solved numerically. For a given QD, the instability corresponds to perturbation with λ having a positive real part. Otherwise, i.e., if $\text{Re}(\lambda) \leq 0$ for all perturbations, then the solution is stable.

In spite of their complex internal structure, dipole and tripole states are stable in a wide subset of their existence domain. Simplified schematics illustrating the main boundaries between stable and unstable solutions are presented in Fig. 1: most of solutions of each type are stable below the corresponding line (blue for dipole QDs and gray for tripole QDs). In Fig. 1 we do not depict some narrow instability areas, where the instability increment is rather small (of order 10^{-3} or below), because it is challenging to detect the borders of all such narrow domains. Representative plots of instability increments vs chemical potential μ_1 are shown in Fig. 5. We have in addition found that the instability becomes strongly inhibited or even disappears completely for solutions situated

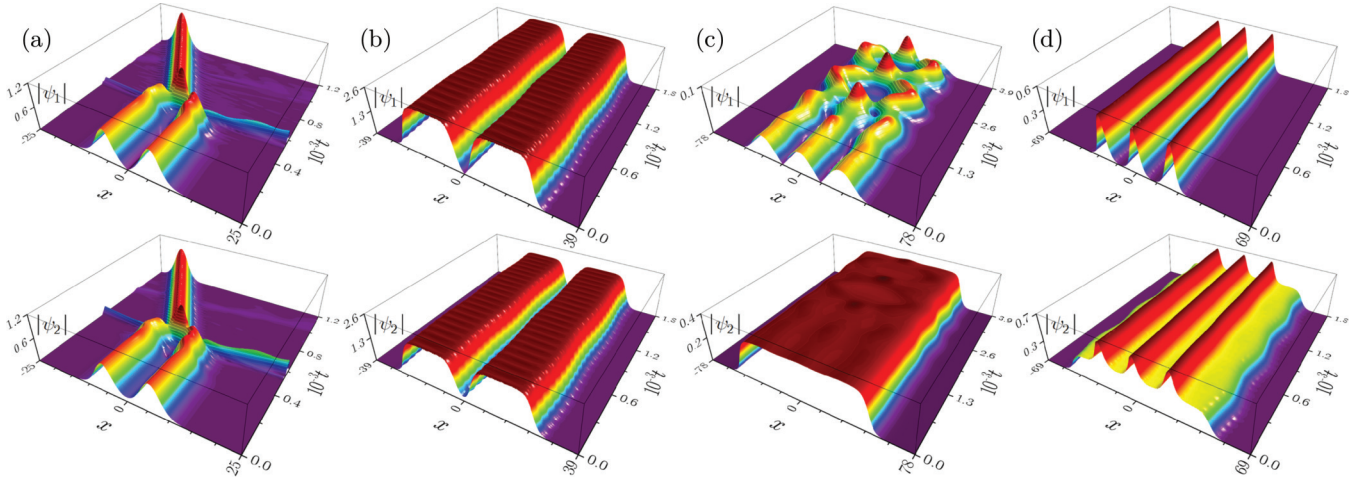


FIG. 6. [(a), (b)] Dynamics of unstable and stable dipole QDs which correspond to solutions with numbers 9 and 15 in Figs. 1 and 4. [(c), (d)] Dynamics of unstable and stable tripole QDs which correspond to solutions with numbers 4 and 10 in Figs. 1, 3, and 4. First and second rows display amplitude of the first [$|\psi_1(x, t)|$] and second [$|\psi_2(x, t)|$] components, respectively.

close to the right boundary of the existence domain. Correspondingly, solutions 1 and 7 are stable, whereas solution 4 features only a “mild” dynamical instability, when time-dependent solutions tend to maintain the internal structure for at least one of components, as opposed to strongly unstable states, which completely lose their structure upon evolution. The difference between “strong” and “mild” instabilities is readily visible from examples of unstable dynamics presented in Fig. 6: a strongly unstable dipole presented in Fig. 6(a) dynamically transforms into a moving fundamental QD, while a weakly unstable tripole illustrated in Fig. 6(c) preserves the shape of the second flattop component and displays quasiperiodic oscillations in the first component. Regarding stable solutions, illustrated in Figs. 6(b) and 6(d), initially introduced random perturbations lead only to small-amplitude oscillations around stationary shapes.

The stability domain for triplets is narrower than for dipoles, as shown in Fig. 1. In addition, for triplets there exists a secondary instability band of finite width situated along the lower boundary of the triangular existence domain. Instability increments in this band are approximately one

order of magnitude smaller than those in the strong instability domain. For simplicity of presentation, we do not show this additional instability area in Fig. 1; however, these instabilities are visible in Fig. 5, where instability increments are plotted as functions of chemical potential μ_1 for two fixed values of μ_2 . At the lower-left boundary of the existence area (which corresponds to the flattop regime), tripole solutions become stable again.

Comparison with monopole solutions. For completeness we briefly discuss monopole, i.e., nodeless, QDs that exist in the mixture with the adopted values of coupling constants. In contrast to multipole QDs, monopole solutions do not undergo fold bifurcations indicated in Fig. 1. Hence, for monopoles the corresponding boundary is absent in Fig. 1, and the domain of their existence on the plane (μ_1, μ_2) is broader. Computing the energy of steady states $\mathcal{E} = \int_{-\infty}^{\infty} [(\partial_x u_1)^2/2 + (\partial_x u_2)^2/2 + E(u_1^2, u_2^2)] dx$ for several representative solutions (two of which are presented in Fig. 7), we observe that for a mixture with fixed numbers of atoms in each species inequalities $\mathcal{E}_m < \mathcal{E}_d < \mathcal{E}_t$ hold, where subscripts m , d , and t stay, respectively, for monopole, dipole, and tripole QDs. Hence, in the energy space monopole and multipole solutions represent ground and excited states, respectively.

Conclusion. We presented a previously unexplored class of multipole quantum droplets in quasi-1D asymmetric Bose-Bose mixtures. Such multipole solutions have no counterparts in the scalar model for a symmetric system and undergo unusual shape transformations within their existence domain. A particularly interesting class of solutions consists of multiple out-of-phase humps in one component coupled to the antidark state in another component. Despite their complex shapes, higher-order excited states are stable in a considerable part of their existence domain.

Acknowledgements. Y.V.K. acknowledges funding by the research project FFUU-2024-0003 of the Institute of Spectroscopy of the Russian Academy of Sciences. The work of D.A.Z. was supported by the Priority 2030 Federal Academic Leadership Program.

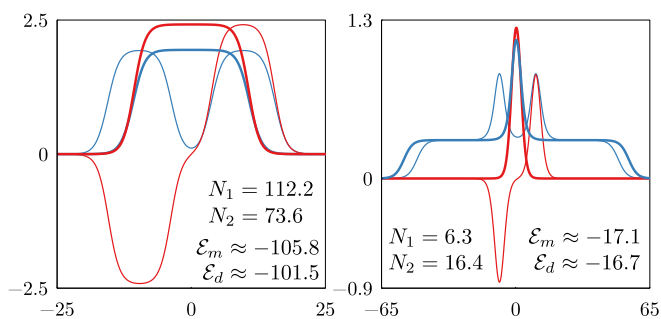


FIG. 7. Two examples of monopole (bold lines) and dipole (thin lines) QDs that share equal numbers of atoms in each species of the mixture. Numbers of atoms in the first (N_1) and second (N_2) species and energies of monopole (\mathcal{E}_m) and dipole (\mathcal{E}_d) solutions are indicated in the plots. Red and blue lines correspond to profiles of the first (u_1) and second (u_2) components.

- [1] T. D. Lee, K. Huang, and C. N. Yang, Eigenvalues and eigenfunctions of a Bose system of hard spheres and its low-temperature properties, *Phys. Rev.* **106**, 1135 (1957).
- [2] D. S. Petrov, Quantum mechanical stabilization of a collapsing Bose-Bose mixture, *Phys. Rev. Lett.* **115**, 155302 (2015).
- [3] D. S. Petrov and G. E. Astrakharchik, Ultradilute low-dimensional liquids, *Phys. Rev. Lett.* **117**, 100401 (2016).
- [4] L. Parisi, G. E. Astrakharchik, and S. Giorgini, Liquid state of one-dimensional Bose mixtures: A quantum Monte Carlo study, *Phys. Rev. Lett.* **122**, 105302 (2019).
- [5] L. Parisi and S. Giorgini, Quantum droplets in one-dimensional Bose mixtures: A quantum Monte Carlo study, *Phys. Rev. A* **102**, 023318 (2020).
- [6] M. Schmitt, M. Wenzel, F. Böttcher, I. Ferrier-Barbut, and T. Pfau, Self-bound droplets of a dilute magnetic quantum liquid, *Nature (London)* **539**, 259 (2016).
- [7] I. Ferrier-Barbut, H. Kadau, M. Schmitt, M. Wenzel, and T. Pfau, Observation of quantum droplets in a strongly dipolar Bose gas, *Phys. Rev. Lett.* **116**, 215301 (2016).
- [8] F. Wächtler and L. Santos, Ground-state properties and elementary excitations of quantum droplets in dipolar Bose-Einstein condensates, *Phys. Rev. A* **94**, 043618 (2016).
- [9] D. Baillie, R. M. Wilson, R. N. Bisset, and P. B. Blakie, Self-bound dipolar droplet: A localized matter wave in free space, *Phys. Rev. A* **94**, 021602(R) (2016).
- [10] L. Chomaz, S. Baier, D. Petter, M. J. Mark, F. Wächtler, L. Santos, and F. Ferlaino, Quantum-fluctuation-driven crossover from a dilute Bose-Einstein condensate to a macrodroplet in a dipolar quantum fluid, *Phys. Rev. X* **6**, 041039 (2016).
- [11] D. Baillie and P. B. Blakie, Droplet crystal ground states of a dipolar Bose gas, *Phys. Rev. Lett.* **121**, 195301 (2018).
- [12] C. R. Cabrera, L. Tanzi, J. Sanz, B. Naylor, P. Thomas, P. Cheiney, and L. Tarruell, Quantum liquid droplets in a mixture of Bose-Einstein condensates, *Science* **359**, 301 (2018).
- [13] G. Semeghini, G. Ferioli, L. Masi, C. Mazzinghi, L. Wolswijk, F. Minardi, M. Modugno, G. Modugno, M. Inguscio, and M. Fattori, Self-bound quantum droplets of atomic mixtures in free space, *Phys. Rev. Lett.* **120**, 235301 (2018).
- [14] P. Cheiney, C. R. Cabrera, J. Sanz, B. Naylor, L. Tanzi, and L. Tarruell, Bright soliton to quantum droplet transition in a mixture of Bose-Einstein condensates, *Phys. Rev. Lett.* **120**, 135301 (2018).
- [15] G. Ferioli, G. Semeghini, L. Masi, G. Giusti, G. Modugno, M. Inguscio, A. Gallemí, A. Recati, and M. Fattori, Collisions of self-bound quantum droplets, *Phys. Rev. Lett.* **122**, 090401 (2019).
- [16] C. D'Errico, A. Burchianti, M. Prevedelli, L. Salasnich, F. Ancilotto, M. Modugno, F. Minardi, and C. Fort, Observation of quantum droplets in a heteronuclear bosonic mixture, *Phys. Rev. Res.* **1**, 033155 (2019).
- [17] L. Cavicchioli, C. Fort, M. Modugno, F. Minardi, and A. Burchianti, Dipole dynamics of an interacting bosonic mixture, *Phys. Rev. Res.* **4**, 043068 (2022).
- [18] Z.-H. Luo, W. Pang, B. Liu, Y.-Y. Li, and B. A. Malomed, A new form of liquid matter: Quantum droplets, *Front. Phys.* **16**, 32201 (2021).
- [19] F. Böttcher, J.-N. Schmidt, J. Hertkorn, K. S. N. Ng, S. D. Graham, M. Guo, T. Langen, and T. Pfau, New states of matter with fine-tuned interactions: quantum droplets and dipolar supersolids, *Rep. Prog. Phys.* **84**, 012403 (2021).
- [20] G. E. Astrakharchik and B. A. Malomed, Dynamics of one-dimensional quantum droplets, *Phys. Rev. A* **98**, 013631 (2018).
- [21] F. K. Abdullaev, A. Gammal, R. K. Kumar, and L. Tomio, Faraday waves and droplets in quasi-one-dimensional Bose gas mixtures, *J. Phys. B: At. Mol. Opt. Phys.* **52**, 195301 (2019).
- [22] S. R. Otajonov, E. N. Tsoy, and F. K. Abdullaev, Stationary and dynamical properties of one-dimensional quantum droplets, *Phys. Lett. A* **383**, 125980 (2019).
- [23] G. C. Katsimiga, S. I. Mistakidis, B. A. Malomed, D. J. Frantzeskakis, R. Carretero-González, and P. G. Kevrekidis, Interactions and dynamics of one-dimensional droplets, bubbles and kinks, *Condens. Matter* **8**, 67 (2023).
- [24] G. C. Katsimiga, S. I. Mistakidis, G. N. Koutsokostas, D. J. Frantzeskakis, R. Carretero-González, and P. G. Kevrekidis, Solitary waves in a quantum droplet-bearing system, *Phys. Rev. A* **107**, 063308 (2023).
- [25] M. Edmonds, Dark quantum droplets and solitary waves in beyond-mean-field Bose-Einstein condensate mixtures, *Phys. Rev. Res.* **5**, 023175 (2023).
- [26] A. Khan and A. Debnath, Quantum droplet in lower dimensions, *Front. Phys.* **10**, 887338 (2022).
- [27] T. Mithun, A. Maluckov, K. Kasamatsu, B. A. Malomed, and A. Khare, Inter-component asymmetry and formation of quantum droplets in quasi-one-dimensional binary Bose gases, *Symmetry* **12**, 174 (2020).
- [28] D. Singh, M. K. Parit, T. S. Raju, and P. K. Panigrahi, Modulational instability in a one-dimensional spin-orbit coupled Bose-Bose mixture, *J. Phys. B: At. Mol. Opt. Phys.* **53**, 245001 (2020).
- [29] S. Gangwar, R. Ravisankar, S. I. Mistakidis, P. Muruganandam, and P. Kumar Mishra, Spectrum and quench-induced dynamics of spin-orbit-coupled quantum droplets, *Phys. Rev. A* **109**, 013321 (2024).
- [30] Y. V. Kartashov, V. M. Lashkin, M. Modugno, and L. Torner, Spinor-induced instability of kinks, holes and quantum droplets, *New J. Phys.* **24**, 073012 (2022).
- [31] S. R. Otajonov, E. N. Tsoy, and F. Kh. Abdullaev, Modulational instability and quantum droplets in a two-dimensional Bose-Einstein condensate, *Phys. Rev. A* **106**, 033309 (2022).
- [32] Y. Li, Z. Chen, Z. Luo, C. Huang, H. Tan, W. Pang, and B. A. Malomed, Two-dimensional vortex quantum droplets, *Phys. Rev. A* **98**, 063602 (2018).
- [33] Y. V. Kartashov, B. A. Malomed, L. Tarruell, and L. Torner, Three-dimensional droplets of swirling superfluids, *Phys. Rev. A* **98**, 013612 (2018).
- [34] Y. V. Kartashov, B. A. Malomed, and L. Torner, Structured hetero-symmetric quantum droplets, *Phys. Rev. Res.* **2**, 033522 (2020).
- [35] Y. V. Kartashov, B. A. Malomed, and L. Torner, Metastability of quantum droplet clusters, *Phys. Rev. Lett.* **122**, 193902 (2019).
- [36] M. N. Tengstrand, P. Stürmer, E. Ö. Karabulut, and S. M. Reimann, Rotating binary Bose-Einstein condensates and vortex clusters in quantum droplets, *Phys. Rev. Lett.* **123**, 160405 (2019).
- [37] L. Dong and Y. V. Kartashov, Rotating multidimensional quantum droplets, *Phys. Rev. Lett.* **126**, 244101 (2021).
- [38] L. Dong, D. Liu, Z. Du, K. Shi, and W. Qi, Bistable multipole quantum droplets in binary Bose-Einstein condensates, *Phys. Rev. A* **105**, 033321 (2022).

- [39] B. Liu, H.-F. Zhang, R.-X. Zhong, X.-L. Zhang, X.-Z. Qin, C. Huang, Y.-Y. Li, and B. A. Malomed, Symmetry breaking of quantum droplets in a dual-core trap, *Phys. Rev. A* **99**, 053602 (2019).
- [40] D. A. Zezyulin, Quasi-one-dimensional harmonically trapped quantum droplets, *Phys. Rev. A* **107**, 043307 (2023).
- [41] Z. Zhou, X. Yu, Y. Zou, and H. Zhong, Dynamics of quantum droplets in a one-dimensional optical lattice, *Commun. Nonlinear Sci. Numer. Simulat.* **78**, 104881 (2019).
- [42] L. Dong, W. Qi, P. Peng, L. Wang, H. Zhou, and C. Huang, Multi-stable quantum droplets in optical lattices, *Nonlinear Dyn.* **102**, 303 (2020).
- [43] I. Morera, G. E. Astrakharchik, A. Polls, and B. Juliá-Díaz, Quantum droplets of bosonic mixtures in a one-dimensional optical lattice, *Phys. Rev. Res.* **2**, 022008(R) (2020).
- [44] X. L. Zhang, X. X. Xu, Y. Y. Zheng, Z. P. Chen, B. Liu, C. Q. Huang, B. A. Malomed, and Y. Y. Li, Semidiscrete quantum droplets and vortices, *Phys. Rev. Lett.* **123**, 133901 (2019).
- [45] Y.-Y. Zheng, S.-T. Chen, Z.-P. Huang, S.-X. Dai, B. Liu, Y.-Y. Li, and S.-R. Wang, Quantum droplets in two-dimensional optical lattices, *Front. Phys.* **16**, 22501 (2021).
- [46] M. R. Pathak and A. Nath, Droplet to soliton crossover at negative temperature in presence of bi-periodic optical lattices, *Sci. Rep.* **12**, 18248 (2022).
- [47] Y. Nie, J.-H. Zheng, and T. Yang, Spectra and dynamics of quantum droplets in an optical lattice, *Phys. Rev. A* **108**, 053310 (2023).
- [48] B. Liu, Y.-X. Chen, A.-W. Yang, X.-Y. Cai, Y. Liu, Z.-H. Luo, X.-Z. Qin, X.-D. Jiang, Y.-Y. Li, and B. A. Malomed, Stable quantum droplets with higher-order vortex in radial lattices, *New J. Phys.* **24**, 123026 (2022).
- [49] Y. V. Kartashov and D. A. Zezyulin, Enhanced mobility of quantum droplets in periodic lattices, *Chaos Solit. Fractals* **182**, 114838 (2024).
- [50] B. Liu, X. Cai, X. Qin, X. Jiang, J. Xie, B. A. Malomed, and Y. Li, Ring-shaped quantum droplets with hidden vorticity in a radially periodic potential, *Phys. Rev. E* **108**, 044210 (2023).
- [51] H. Huang, H.-C. Wang, G. Chen, M. Chen, C. S. Lim, and K.-C. Wong, Stable quantum droplets with higher-order vortex in radial lattices, *Chaos Solit. Fractals* **168**, 113137 (2023).
- [52] F. Minardi, F. Ancilotto, A. Burchianti, C. D'Errico, C. Fort, and M. Modugno, Effective expression of the Lee-Huang-Yang energy functional for heteronuclear mixtures, *Phys. Rev. A* **100**, 063636 (2019).